

---

# MECHANISM LEARNING: REVERSE CAUSAL INFERENCE IN THE PRESENCE OF MULTIPLE UNKNOWN CONFOUNDING THROUGH FRONT-DOOR CAUSAL BOOTSTRAPPING

---

**Jianqiao Mao**

School of Computer Science  
University of Birmingham  
Birmingham, B15 2TT  
jxm1417@student.bham.ac.uk

**Max A. Little**

School of Computer Science  
University of Birmingham  
Birmingham, B15 2TT  
maxl@mit.edu

October 29, 2024

## ABSTRACT

A major limitation of machine learning (ML) prediction models is that they recover associational, rather than causal, predictive relationships between variables. In high-stakes automation applications of ML this is problematic, as the model often learns spurious, non-causal associations. This paper proposes *mechanism learning*, a simple method which uses front-door causal bootstrapping to deconfound observational data such that any appropriate ML model is forced to learn predictive relationships between effects and their causes (reverse causal inference), despite the potential presence of multiple unknown and unmeasured confounding. Effect variables can be very high dimensional, and the predictive relationship nonlinear, as is common in ML applications. This novel method is widely applicable, the only requirement is the existence of a mechanism variable mediating the cause (prediction target) and effect (feature data), which is independent of the (unmeasured) confounding variables. We test our method on fully synthetic, semi-synthetic and real-world datasets, demonstrating that it can discover reliable, unbiased, causal ML predictors where by contrast, the same ML predictor trained naively using classical supervised learning on the original observational data, is heavily biased by spurious associations. We provide code to implement the results in the paper, online.

**Keywords** Causal machine learning · front-door criterion · reverse causal inference · medical imaging

## 1 Introduction

In recent years, machine learning (ML) has shown promising performance in many applications, to name but a few: disease diagnosis (Ahsan et al., 2022), automatic driving (Alam and Praveen, 2021), and adaptive control (Mao et al., 2023; Zamfirache et al., 2023). However, one of the major limitations of applying ML methods in critical, high-stakes applications such as decision-making in medicine, is their “causal blindness” (Little and Badawy, 2019), that is, ML models are, by design, pattern-recognition algorithms which learn potentially spurious, non-causal associations between the feature and target variables.

One solution to this blindness is to train ML algorithms on experimental (interventional) data which eliminates unwanted associations, capturing only the desired causal relationships. Unfortunately, such data, collected

---

The experiment code, mechanism learning Python package installation and usage instructions for this study can be accessed through the [GitHub repository](#).

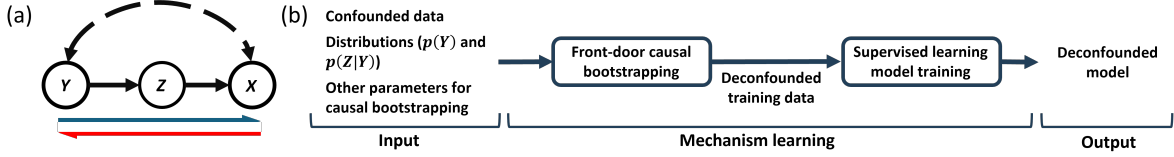


Figure 1: Mechanism learning (b) is a novel, simple and widely applicable solution to the problem of reverse causal inference in the presence of multiple unknown confounding, using arbitrary supervised ML algorithms to predict nonlinear effect-cause relationships from potentially high-dimensional effects. The causal scenario is represented by the ubiquitous *front-door* causal graph (a). There are multiple, unmeasured/unknown confounding paths between  $Y$  and  $X$  (bi-directed, dashed arrow). The classic causal inference direction is the causal path from  $Y$  to  $X$  via  $Z$  (blue half arrow); reverse causal inference infers causes  $Y$  from effects  $X$  (red half arrow).

under well-controlled experimental settings, is normally expensive and comparably small-scale, which may not meet the heavy sample size demands of modern, sophisticated ML models (Zhao et al., 2023). Moreover, controlled experiments may be physically impossible or unethical to conduct, for instance in global climate science and macroeconomics. By contrast, observational data is now easier and cheaper to collect due to advances in data collection, storage and sensing technology. Nevertheless, observational data can be easily corrupted by known or latent confounding factors (Ming et al., 2022). Interestingly, the prediction performance of ML models trained on confounded data may be *significantly over-estimated* and fail to hold when confounders are no longer present, as often happens in practical deployment settings. The primary reason for this overestimate is simple – association does not generally imply causation – except under special circumstances. In terms of Pearl’s *do-calculus*,  $p(x|do(y)) \neq p(x|y)$  for most situations where observational data alone is available (Pearl, 2009).

Various *causal inference* (CI) methods have been proposed to identify and quantify causal effects from observational data, such as instrumental variables (Baiocchi et al., 2014), propensity score matching (Yang et al., 2021) and advanced ML algorithms such as the causal forest predictor (Wager and Athey, 2018). A systematic approach to nonparametric structural causal inference involves the integration of *structural causal models* (SCM), *do-calculus* and related analytical methods (Pearl, 2009; Richardson et al., 2023). A commonly-encountered causal scenario, called *front-door confounding*, occurs where one or more latent (unmeasured) variables introduce spurious causal influence between both cause ( $Y$ ) and effect ( $X$ ) variables and a *mechanism* (a.k.a. mediator in some texts) ( $Z$ ) variable exists between cause and effect (Figure 1). In this situation, the cause-effect relationship is *identifiable* using *front-door adjustment* (Pearl, 2009) from the observational data, so we can quantitatively estimate the causal effect of  $Y$  on  $X$  without the need to carry out any interventional experiments.

These existing CI methods, although useful, are generally not applicable to high-dimensional variables or estimating nonlinear relationships, while ML predictors are. Supervised ML predictions are typically made in the *reverse causal* direction, that is, counter to the generative causal arrow, predicting causes from effects, unlike traditional CI where effects of causes are predicted (for instance, average treatment effects). For example, in the front-door setting (Figure 1(a)), the cause  $Y$  can be some diagnostic category and the effect  $X$  may be some high-dimensional features such as images or other digital measurements. The ML prediction goal is to use the features to predict the diagnostic category. Here, the variable  $Z$  could represent some *disease-dependent mechanism* that “explains” the diagnostic category for given digital images.

This report proposes *mechanism learning*, a novel method that enables arbitrary supervised ML models to perform reverse causal inference for the front-door confounding scenario without altering the ML model. Such an ML model trained using mechanism learning, will be an estimate of the true, causal, feature-label relationship, *unbiased by any spurious associations* between these variables. Mechanism learning is widely applicable: specifically, to any situation where, in addition to label and feature data, there exists data for the mechanism. For example, in radiology, there are unique morphological features caused by different diseases which lead to specific patterns in the digital images, while many unmeasured and/or unknown confounders exist such as the imaging device protocol and patient demographics which simultaneously influence both the

diagnostic category and the images. The basis for mechanism learning is *front-door causal bootstrapping* (CB) presented in [Little and Badawy \(2019\)](#), a weighted bootstrap which deconfounds the observational data so as to approximate the distribution of non-confounded, interventional data.

To demonstrate the effectiveness of this novel method, firstly, we train simple ML models using mechanism learning on a set of synthetic and semi-synthetic datasets with explicitly constructed mechanism variables. This experiment, where we have full control over the generative model of the data, clearly shows how ML models trained using mechanism learning are more robust to unmeasured confounding than the same ML models trained using classical supervised learning. Secondly, we use mechanism learning to train a sophisticated supervised ML model on a real-world dataset for the medical problem of intracranial hemorrhage (ICH) detection using computed tomography (CT) images ([Hssayeni et al., 2020](#)). A challenge for mechanism learning in this setup is the high-dimensionality of the mechanism variable (segmented hemorrhage areas labeled by a group of professional radiologists). By obtaining a low-dimensional representation of the mechanism variable, we are able to demonstrate that the same ML model classically trained using supervised learning, substantially overfits to the unknown confounding in the dataset such that its performance collapses when this confounding is removed by CB. By contrast, the ML model trained using mechanism learning, has highly stable performance across both confounded and deconfounded settings. This provides strong evidence that, through mechanism learning, the ML algorithm has learned to predict the true, causal image-category relationship, rather than any other spurious relationship in the original dataset.

Next, we describe the proposed mechanism learning method in detail.

## 2 Mechanism learning

As discussed above (see also Fig. 1), the core of this method is the use of causal bootstrapping ([Little and Badawy, 2019](#)) applied to the front-door SCM ([Pearl, 2009](#); [Glynn and Kashin, 2013](#); [Bellemare et al., 2024](#)). CB thus deconfounds the observational data before it is used to train a standard supervised learning model. The following sections recall the theoretical basis of front-door CB.

### 2.1 Bootstrap weights for front-door interventional distributions

A formal definition of the well-known *front-door criterion* is given by the following:

**Definition 2.1** (Front-door criterion ([Pearl, 2009](#))). Given variables  $Y$ ,  $X$  and  $Z$ , the causal effect from the cause  $Y$  to the effect  $X$  is identifiable if:

1. The mechanism  $Z$  intercepts all directed paths from  $Y$  to  $X$ .
2. There are no unmeasured confounders between  $Y$  and  $Z$ .
3. All backdoor paths from  $Z$  to  $X$  are blocked by  $Y$ .

For a set of variables that satisfy this criterion, we can use do-calculus to compute the interventional distribution ([Pearl, 2010](#)):

$$\begin{aligned} p(x, y', z | do(y)) &= p(x | y', z) p(y') p(z | y) \\ &= p(x, y', z) \frac{p(z | y)}{p(z | y')}, \end{aligned} \tag{1}$$

where the random variable  $Y'$  is a copy of variable  $Y$  which arises during the application of do-calculus.

The joint distribution  $p(x, y', z)$  can be replaced by any *kernel density estimator* (KDE):

$$p(x, y', z) \approx \frac{1}{N} \sum_{n \in \mathcal{N}} K[x - x_n] K[y' - y_n] K[z - z_n], \tag{2}$$

where  $K[\cdot]$  is some kernel density function,  $N$  is the sample size,  $x_n$ ,  $y_n$  and  $z_n$  are realizations of the effect variable  $X$ , the cause variable  $Y$  and the mechanism variable  $Z$ , respectively. Inserting (2) into (1), we

obtain:

$$p(x, y', z | do(y)) \approx \frac{1}{N} \sum_{n \in \mathcal{N}} K[x_n - x] K[z - z_n] K[y' - y_n] \frac{p(z|y)}{p(z|y')}. \quad (3)$$

The variables  $Y'$  and  $Z$  are not of interest to the cause-effect relationship, thus we marginalize them out:

$$p(x | do(y)) \approx \frac{1}{N} \int \int \sum_{n \in \mathcal{N}} K[x_n - x] K[z - z_n] K[y' - y_n] \frac{p(z|y)}{p(z|y')} dy' dz. \quad (4)$$

Since the distribution and kernel functions are non-negative by construction, Tonelli's theorem (Folland, 1999) shows that the summation and integration above can be interchanged. So, we can rewrite (4) as:

$$p(x | do(y)) \approx \frac{1}{N} \sum_{n \in \mathcal{N}} K[x_n - x] \int \int K[z - z_n] K[y' - y_n] \frac{p(z|y)}{p(z|y')} dy' dz, \quad (5)$$

Therefore, the front-door CB weights are given by:

$$w_n = \frac{1}{N} \int \int K[z - z_n] K[y' - y_n] \frac{p(z|y)}{p(z|y')} dy' dz. \quad (6)$$

The conditional distribution  $p(z|y)$  may typically be estimated from the observational data using a suitable estimator, unless prior knowledge is available.

*Reproducing Kernel Hilbert Spaces* (RKHS) functions have the *reproducing property*, where:

$$\langle p, K[x, \cdot] \rangle = \int p(x') K[x - x'] dx' = p(x), \quad (7)$$

and, given an RKHS kernel for the KDE, we can use this property to evaluate the inner integrals in (6). Finally, this means the weights  $w_n$  are essentially evaluated at each observational data point:

$$\begin{aligned} w_n &= \frac{p(z|y)}{N p(z|y')} \Big|_{z=z_n, y'=y_n} \\ &= \frac{p(z_n|y)}{N p(z_n|y_n)}. \end{aligned} \quad (8)$$

For bootstrap resampling purposes, the resulting interventional distribution is given by:

$$p(x | do(y)) \approx \sum_{n \in \mathcal{N}} K[x_n - x] w_n, \quad (9)$$

where an appropriate kernel  $K[\cdot]$  is used for the effect  $X$ . For example, for discrete data, this would be the Kronecker delta, and for continuous data the (potentially multi-dimensional) Dirac delta, which results in the “standard” causal bootstrap, which is just a weighted form of the usual bootstrap distribution (Tibshirani and Efron, 1993). Non-Dirac kernels lead to *kernel* causal bootstraps.

Sample efficiency for the front-door CB remains tractable even if the effect variable  $\mathbf{X}$  is high-dimensional, a common occurrence in many ML applications. This is because we do not need to estimate any marginal or joint distributions associated with the high-dimensional features  $\mathbf{X}$ . This implies that accurate front-door CB weights can be estimated even for relatively small datasets  $\mathcal{D}$ , where accurate distribution estimation for all joint variables in the model would generally be infeasible.

## 2.2 Front-door causal bootstrap

Since do-calculus allows identification of the interventional distribution, the front-door CB weights encode that distribution for bootstrapping, even if there are multiple unknown or unmeasured confounders that

connect causal paths between  $Y$  and  $X$ . With the computed weights, it is then possible to resample a new and deconfounded dataset  $\hat{\mathcal{D}}$  as the training data for classical supervised learning.

This gives us the front-door causal bootstrap (Algorithm 1). Since, in an interventional distribution such as  $p(\mathbf{x} | do(y))$ , the actual interventional value  $y$  is chosen freely, there is a choice for its distribution. For example, setting  $\hat{y}_m = y_n$  and  $M = N$  ensures that the distribution of  $\hat{Y}$  is an exact match for the observational distribution  $Y$ . In some situations this is useful since it ensures no distribution shift between the original observational and bootstrapped interventional data. However, other distributions for the intervention (for example, the uniform distribution) might be preferable in certain scenarios such as imbalanced class settings and general regression tasks.

---

**Algorithm 1** Front-door causal bootstrap for mechanism learning

---

**Input:**  $N$  samples  $\mathcal{D} = (\mathbf{x}_n, y_n, \mathbf{z}_n)$  and  $n \in \mathcal{N} = \{1, 2, \dots, N\}$  of potentially confounded observational data from arbitrary feature data  $\mathbf{X}$ ; prediction target  $Y$  and mechanism  $\mathbf{Z}$  with sample spaces  $\Omega_{\mathbf{X}}$ ,  $\Omega_Y$  and  $\Omega_{\mathbf{Z}}$ , respectively; bootstrap size  $M$  and interventions for each bootstrapped sample  $\hat{\mathbf{y}} = [\hat{y}_1, \hat{y}_2, \dots, \hat{y}_M]$ , for  $m \in \mathcal{M} = \{1, 2, \dots, M\}$ .

**Output:**  $M$  deconfounded samples  $\hat{\mathcal{D}} = (\mathbf{x}_m, y_m)$ , approximating samples from  $p(\mathbf{x} | do(y))$

**Steps:**

**if** Distribution  $p(z, y)$  is unknown **then:**

Estimate  $p(z, y)$  from  $\mathcal{D}$  to compute  $p(z | y)$ .

**else:**

Use the true conditional distribution  $p(z | y)$ .

**end if**

**for** each  $m \in \mathcal{M}$  **do:**

Produce new sample  $(\mathbf{x}_i, \hat{y}_m) \in \hat{\mathcal{D}}$ , where index  $i$  is selected from  $\mathcal{N}$  with weights:

$$w_i = \frac{p(z_i | \hat{y}_m)}{N p(z_i | y_i)}$$

**end for**

---

### 3 Tests with fully- and semi-synthetic generative models

In this section, we compare the performance of simple supervised ML models with and without mechanism learning, on data for which the generating model is known. As a shorthand, below we call the ML model trained with mechanism learning the *deconfounded* model and the classical supervised model the *confounded* model.

Two fully synthetic datasets were generated for classification (categorical prediction target  $Y$ ) and regression (continuous prediction target  $Y$ ). For the semi-synthetic dataset, we modify the MNIST dataset (LeCun et al., 1998) by adding a background brightness confounder under the front-door causal setting. For generative model details, see Appendix 5.

As a showcase, we discuss the semi-synthetic background-MNIST dataset to demonstrate how unmitigated confounding in the training data can lead to a causally biased and therefore unreliable, ML model. Note that, this bias cannot be detected from investigation of the test set accuracy alone. In the confounded dataset images of digit “6” tend to have brighter backgrounds than images of digit “2”, but this confounding effect is not observed for the non-confounded dataset (Figure 2). A standard supervised classifier trained on the confounded MNIST dataset is likely to make predictions based on the input image’s average brightness rather than the handwriting digit’s actual shape because the brightness feature is strongly associated with the label. Thus, any supervised learning algorithm will use this spurious brightness information to maximize prediction accuracy. However, this brightness information is not what we expect the classifier to learn; should the predictor be applied to data without this brightness confounder, it would be of no use, despite the apparently high out-of-sample accuracy of the predictor.



Figure 2: Example digits from the confounded (a) and non-confounded background-MNIST datasets (b). The background brightness is manipulated so that it is a confounding factor correlated with the digit category, such that digit “6” has, on average, brighter background than digit “2” (a). Through front-door causal bootstrapping (b), the brightness-digit association is randomized, thereby simulating data collected from a controlled experiment in which the digit category is selected independent of all possible confounding factors.

### 3.1 Test results: synthetic classification dataset

Using a simple linear-kernel support vector machine (SVM) classifier, we compare predictive decision boundaries trained with/without mechanism learning. The confounded SVM, trained using classical supervised learning, is severely affected by the confounder (Figure 3), whose decision boundary conflates the true class with the implied confounder boundaries. By contrast, the decision boundary of the deconfounded SVM closely matches the true class boundary which nullifies the influence of the confounder. Therefore, the deconfounded SVM, trained using mechanism learning, captures the desired causal relationship between features and prediction target.

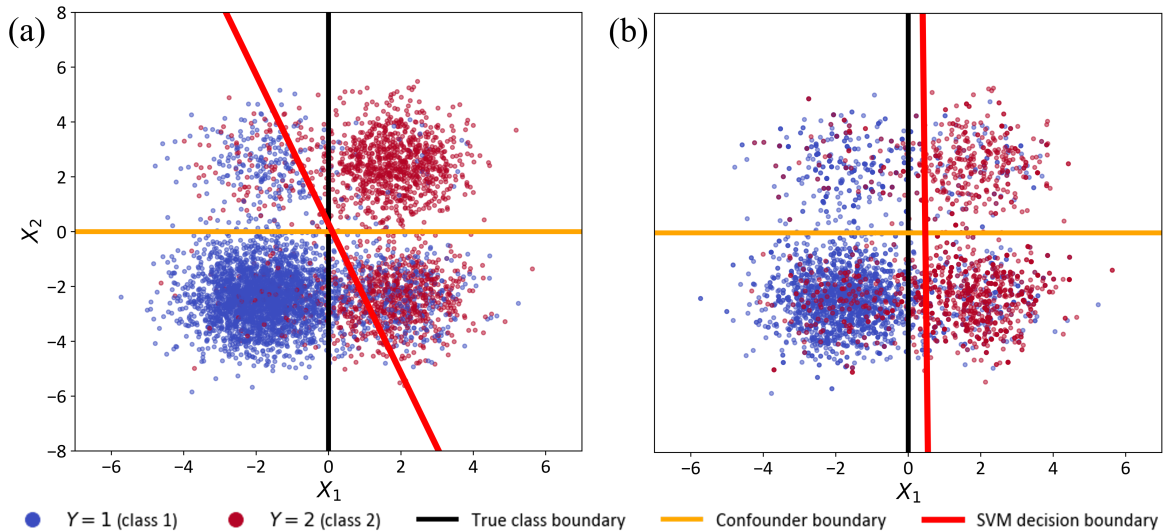


Figure 3: Comparing classifiers trained using (a) classical supervised learning and (b) mechanism learning, on the synthetic classification dataset. With confounded data (a), class 1 samples tend to concentrate in the bottom left region, with class 2 samples in the top right. The SVM classifier’s decision boundary mixes the true with the confounding boundary. By contrast, after applying front-door CB (b) the confounding factor has been nullified, such that the SVM decision boundary is close to the true class boundary.

In terms of performance evaluation metrics (Table 1) the SVM trained using mechanism learning, exceeds the SVM trained using classical supervised learning on the non-confounded dataset by 5% accuracy, retaining stable predictive accuracy across both confounded and non-confounded datasets. On the contrary, although the classical supervised SVM performs about as well as the deconfounded SVM in the confounded dataset, its performance declines significantly on the non-confounded dataset. This is because classical supervised learning is biased by the influence of confounding, reporting misleading accuracy on the original (confounded) test set.

### 3.2 Test results: synthetic regression dataset

Training two simple univariate linear regression models, we again compare predictive performance using classical versus mechanism learning (Figure 4). In this regression problem, the deconfounded dataset is sampled using a uniformly distributed interventional variable, rather than by matching the distribution of the observational cause variable. Classical regression leads to a model whose regression line has much smaller slope than the true, causal slope between feature  $X$  and target  $Y$ .

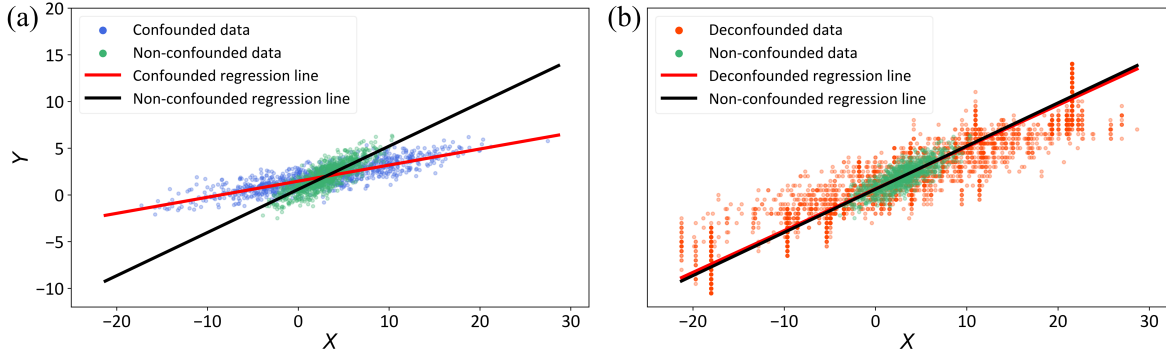


Figure 4: Comparison of the trained regression models with/without **mechanism learning**. (a) compares the confounded and non-confounded regression lines and their corresponding datasets, where the confounded regression line has a smaller slope due to the confounder  $U$ . (b) compares the deconfounded and non-confounded regression lines with their corresponding datasets, where the deconfounded regression line is closer to the non-confounded one.

In terms of prediction error (Table 1), the deconfounded model trained using mechanism learning has smaller error (by around 0.3 units) than the regression model trained using supervised learning, when both are applied to the nonconfounded test dataset. Although the confounded linear regression model exceeds the performance of the deconfounded one on the confounded test set, this is not a stable and reliable regression relationship which significantly depends on the confounding factor. However, this is not the intended true causal relationship that we wish the model to learn.

### 3.3 Test results: semi-synthetic background-MNIST dataset

A simple ML classification model achieves fairly high prediction accuracy at separating digits (Table 1) on background-brightness confounded data, regardless of whether the ML model is trained using classical supervised or mechanism learning. However, on non-confounded data, the ML model trained using mechanism learning exceeds the performance of the classical supervised model by a significant margin. This is good evidence that the classical model is heavily biased by the strong confounding i.e. the background brightness. By contrast, the model trained using mechanism learning makes unbiased causal predictions about the shape of the digits, which are robust to background brightness.

## 4 Application to real-world data: ICH detection with CT scans

The experiments above show that an ML model trained using classical supervised learning on an observational dataset tends to capture biased relationships between the feature and target variable and loses robustness and reliability due to the presence of unmeasurable confounders. Mechanism learning overcomes this failure to a significant degree. We now turn to tests on real-world data, where the data generating process is unknown.

ICH is a life-threatening medical condition but difficult and time-consuming to diagnose (Caceres and Goldstein, 2012). The current clinical approach to ICH detection is based on radiologist examination of CT scans. Many efforts have been made to develop automatic, efficient, ML-assisted tools for ICH diagnosis (Hssayeni et al., 2020; Wang et al., 2021). However, data from CT scans labeled with an ICH diagnostic

| Dataset                         | Machine learning model | Performance metric | Mechanism learning? | Test data  |                |
|---------------------------------|------------------------|--------------------|---------------------|------------|----------------|
|                                 |                        |                    |                     | Confounded | Non-confounded |
| Synthetic classification        | Linear SVM             | Accuracy           | True                | 0.85       | 0.83           |
|                                 |                        |                    | False               | 0.85       | 0.78           |
| Semi-synthetic background-MNIST | KNN                    | Accuracy           | True                | 0.93       | 0.92           |
|                                 |                        |                    | False               | 0.95       | 0.74           |
| Synthetic regression            | Linear regression      | RMSE               | True                | 2.00       | 0.79           |
|                                 |                        |                    | False               | 0.77       | 1.08           |

Table 1: Test results comparing classical supervised against mechanism learning on fully- and semi-synthetic datasets, where the data is generated from known structural models.

category collected as a result of routine clinical practice, can be severely confounded by many unmeasurable or unknown factors, such as the imaging device’s hardware or settings, hospital usage protocols, the patient’s age or gender, and combinations of all the above factors. Developing reliable ML-based detection algorithms using this dataset, is difficult as a result.

#### 4.1 Dataset description and processing

For this dataset, the cause variable is the six-class diagnostic ICH category, the mechanism variable is the segmentation of the potential hemorrhage region in the CT scans, and the effect variable is the high-dimensional CT images (Figure 5).

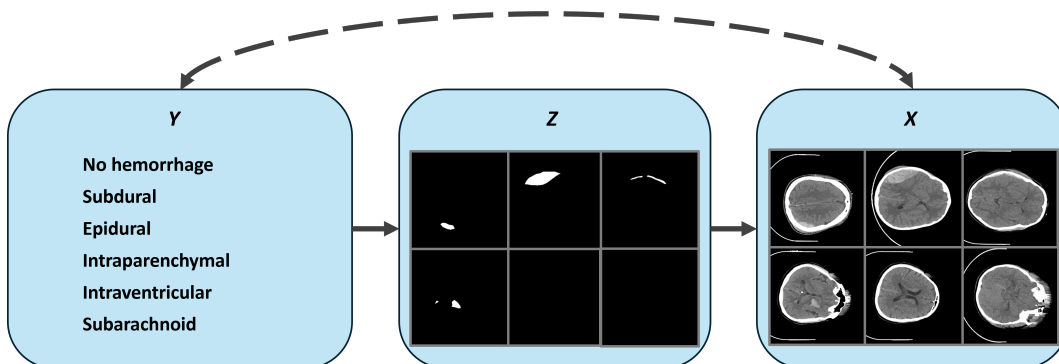


Figure 5: Front-door structural causal model for the real-world ICH dataset (Hssayeni et al., 2020), for the purposes of mechanism learning. The cause variable  $Y$  represents diagnostic category; mechanism variable  $Z$  represents hemorrhage region label, and the effect variable  $X$  are the digital CT scans.

There are 82 sets of CT scans including 36 slices for each set. There are five abnormal ICH categories: intraventricular, intraparenchymal, subarachnoid, epidural and subdural, plus a normal category representing no hemorrhage. Each slice is consensus region-labeled by two radiologists, annotating the hemorrhage type. The radiologists have no access to the clinical history of the patients.

All the original CT scan slices and labeled hemorrhage region images are  $512 \times 512$  pixel grayscale images whose pixel value range is  $[0, 255]$ . These are downsampled to  $128 \times 128$  pixels and normalized to the range  $[0, 1]$  to save computational effort. Some CT scan slices contain no meaningful information, for example, some slices are out of the brain area of interest. We delete these samples by a semi-manual selection process: if a slice’s black area is more than 90%, they are filtered out; if a slice’s black area is more than 80%, we determine if this slice should be kept on a case-by-case basis.

Investigating the distributions of the diagnostic categories shows a severe class imbalance where most of the slices are labeled as “no hemorrhage” (more than 80%) and some abnormal categories have very few samples (less than 2%). Therefore, we re-balance the sample sizes based on class, in the following way.

For the deconfounded data, we bootstrap more samples for the minority classes and fewer samples for the majority class using front-door CB. To ensure fair comparisons, random oversampling/undersampling is used to resample the confounded dataset, keeping exactly the same size for each category as the front-door CB does.

## 4.2 Mechanism embedding

To apply mechanism learning, we need to estimate the unknown joint distribution of the mechanism and cause variables,  $p(x, y)$ . However, accurate distribution estimations for such high-dimensional mechanism variable is impractical. Therefore, we design a ResNet-based encoder-decoder model to extract a 10-dimensional embedding of the labeled ICH regions (Figure 6). A combined loss function takes the weighted sum of the pixel-wise cross-entropy loss and structure similarity loss. Data augmentation is also applied to input images by random rotation, shifting, flipping and zooming. Investigating the resulting embeddings shows that there is an all-zero dimension, which is dropped in later usage.

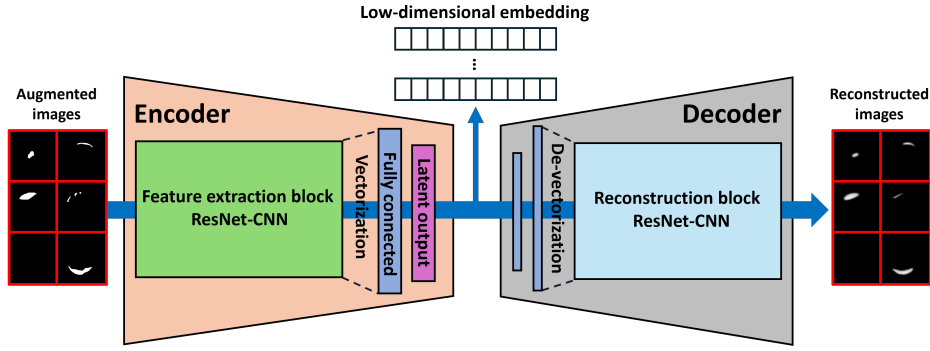


Figure 6: Encoder-decoder for mechanism variable embedding in the real-world ICH dataset. The 10-dimensional output of the encoder is used as the low-dimensional representation for the hemorrhage region images. In the encoder, a 5-layer ResNet-CNN block with alternating convolutional and pooling layers extracts features of input hemorrhage region images. These features are then vectorized as the input of a fully connected layer, followed by a latent representation output layer. A corresponding structure is used in the decoder but the pooling layers are substituted by convolutional layers to reconstruct the image based on the low-dimensional embeddings.

## 4.3 Non-confounded test data synthesis and evaluation

Unlike the case with synthetic data, we do not have the non-confounded data so as to make model performance comparisons. Instead, we assume that the front-door CB process produces deconfounded data which effectively mimics real-world ICH data without confounders. We split the deconfounded front-door CB data into train and test sets. By identifying the samples which are resampled during the bootstrapping process, we ensure that the training and test sets are fully disjoint, by randomly sampling without replacement from the original sample indices. In this way, we ensure the original, unique data samples are split in the same way between both confounded and deconfounded training sets, as with the test sets. To retain consistency, in terms of class (diagnostic category) distribution and dataset size, with the front-door CB deconfounded datasets, the original confounded training and test sets are resampled by random oversampling/undersampling.

Next, we train two ResNet-CNNs models with and without mechanism learning, and compute out-of-sample ICH class prediction performance (Table 2). In agreement with theory and synthetic experiments, the ResNet-CNN trained using mechanism learning, significantly exceeds the performance of the same ResNet-CNN trained using classical supervised learning, when tested on the independent, deconfounded test set. Furthermore, the ResNet-CNN trained using mechanism learning, has similar predictive performance on the confounded test dataset as with the deconfounded test dataset.

Our interpretation of this finding is that the model trained with mechanism learning largely nullifies the effect of unknown confounding factors. By contrast, the confounded model’s performance dramatically degrades on the independent deconfounded test set. Note that here, our aim is not to produce the most complex predictor (there could indeed be ML predictors which achieve higher accuracy for this problem); instead the aim of this experiment is to demonstrate the effectiveness of mechanism learning by comparison to classical supervised learning.

| Model      | Mechanism learning? | Training Data | Test data   |                |
|------------|---------------------|---------------|-------------|----------------|
|            |                     |               | Confounded  | Non-confounded |
| ResNet-CNN | True                | Deconfounded  | 0.87 (0.04) | 0.84 (0.03)    |
|            | False               | Confounded    | 0.91 (0.04) | 0.64 (0.02)    |

Table 2: Average class prediction accuracy in 30 repeated experiments on the real-world ICH dataset (Hssayeni et al., 2020). Prediction performance (average accuracy with the corresponding standard deviation shown in brackets) comparison between the same ResNet-CNN model trained with mechanism learning or without mechanism learning (using classical supervised learning), tested on independent confounded and deconfounded datasets.

## 5 Conclusion and Discussion

In this paper we propose mechanism learning, a simple, novel method to train existing supervised ML prediction models which are robust to the spurious associations which are common to real-world observational datasets. The method is based on front-door causal bootstrapping: the use of do-calculus and RKHS-based KDEs, applied to the front-door structural causal model to bootstrap from the interventional distribution of direct causal path between feature data and prediction target. In this way, the ML model makes reverse causal inferences of prediction target from feature data, with only access to the confounded observational data.

Through simulations on synthetic data and application to a real-world dataset, we demonstrated the robustness of the novel training method to potential confounding, confirming that the method is effective at recovering the direct causal, rather than any spurious, influences. In our view, this represents a significant advance towards the deployment of ML methods which can make both accurate and reliable predictions. In high-stakes applications such as medical decision-making or safety-critical engineering systems, predictive accuracy of ML models is not everything: much more important is robustness/reliability, which can be afforded through the appropriate adaptation of structural causal inference to supervised ML modelling, as we demonstrate here.

## References

- Md Manjurul Ahsan, Shahana Akter Luna, and Zahed Siddique. Machine-learning-based disease diagnosis: A comprehensive review. In *Healthcare*, volume 10, page 541. MDPI, 2022.
- Afroj Alam and Sheeba Praveen. A review of automatic driving system by recognizing road signs using digital image processing. *Journal of Informatics Electrical and Electronics Engineering (JIEEE)*, 2(2): 1–9, 2021.
- Jianqiao Mao, Ryan Grammenos, and Konstantinos Karagiannis. Data analysis and interpretable machine learning for hvac predictive control: A case-study based implementation. *Science and Technology for the Built Environment*, 29(7):698–718, 2023.
- Iuliu Alexandru Zamfirache, Radu-Emil Precup, Raul-Cristian Roman, and Emil M Petriu. Neural network-based control using actor-critic reinforcement learning and grey wolf optimizer with experimental servo system validation. *Expert Systems with Applications*, 225:120112, 2023.
- Max A Little and Reham Badawy. Causal bootstrapping. *arXiv preprint arXiv:1910.09648*, 2019.
- Wayne Xin Zhao, Kun Zhou, Junyi Li, Tianyi Tang, Xiaolei Wang, Yupeng Hou, Yingqian Min, Beichen Zhang, Junjie Zhang, Zican Dong, et al. A survey of large language models. *arXiv preprint arXiv:2303.18223*, 2023.

- Yifei Ming, Hang Yin, and Yixuan Li. On the impact of spurious correlation for out-of-distribution detection. In *Proceedings of the AAAI conference on artificial intelligence*, volume 36, pages 10051–10059, 2022.
- J Pearl. *Causality*. Cambridge university press, 2009.
- Michael Baiocchi, Jing Cheng, and Dylan S Small. Instrumental variable methods for causal inference. *Statistics in medicine*, 33(13):2297–2340, 2014.
- Siyun Yang, Elizabeth Lorenzi, Georgia Papadogeorgou, Daniel M Wojdyla, Fan Li, and Laine E Thomas. Propensity score weighting for causal subgroup analysis. *Statistics in medicine*, 40(19):4294–4309, 2021.
- Stefan Wager and Susan Athey. Estimation and inference of heterogeneous treatment effects using random forests. *Journal of the American Statistical Association*, 113(523):1228–1242, 2018.
- Thomas S Richardson, Robin J Evans, James M Robins, and Ilya Shpitser. Nested markov properties for acyclic directed mixed graphs. *The Annals of Statistics*, 51(1):334–361, 2023.
- Murtadha Hssayeni, M Croock, A Salman, H Al-khafaji, Z Yahya, and B Ghoraani. Computed tomography images for intracranial hemorrhage detection and segmentation. *Intracranial hemorrhage segmentation using a deep convolutional model*. *Data*, 5(1):14, 2020.
- Adam Glynn and Konstantin Kashin. Front-door versus back-door adjustment with unmeasured confounding: Bias formulas for front-door and hybrid adjustments. In *71st Annual Conference of the Midwest Political Science Association*, volume 3, 2013.
- Marc F Bellemare, Jeffrey R Bloem, and Noah Wexler. The paper of how: Estimating treatment effects using the front-door criterion. *Oxford Bulletin of Economics and Statistics*, 86(4):951–993, 2024.
- Judea Pearl. An introduction to causal inference. *The international journal of biostatistics*, 6(2), 2010.
- Gerald B Folland. *Real analysis: modern techniques and their applications*, volume 40. John Wiley & Sons, 1999.
- Robert J Tibshirani and Bradley Efron. An introduction to the bootstrap. *Monographs on statistics and applied probability*, 57(1):1–436, 1993.
- Yann LeCun, Léon Bottou, Yoshua Bengio, and Patrick Haffner. Gradient-based learning applied to document recognition. *Proceedings of the IEEE*, 86(11):2278–2324, 1998.
- J Alfredo Caceres and Joshua N Goldstein. Intracranial hemorrhage. *Emergency medicine clinics of North America*, 30(3):771–794, 2012.
- Xiyue Wang, Tao Shen, Sen Yang, Jun Lan, Yanming Xu, Minghui Wang, Jing Zhang, and Xiao Han. A deep learning algorithm for automatic detection and classification of acute intracranial hemorrhages in head ct scans. *NeuroImage: Clinical*, 32:102785, 2021.

## Appendix A. Data generation processes for semi- and fully-synthetic datasets

### A.1. Synthetic classification data

For the synthetic classification data, the cause  $Y$  and the (latent) confounder  $U$  are (conditional) Bernoulli random variables, whose sample spaces are  $\Omega_Y, \Omega_U = \{1, 2\}$ . The mechanism  $Z$  and effect  $\mathbf{X}$  are (multi-dimensional) Gaussian random variables whose parameters depend on their parent variables. Formally, their dependency is:

$$\begin{aligned}
 U &\sim \text{Bernoulli}(p = 0.25) \\
 Y|U &\sim \text{Bernoulli}(p = q_y(u)) \\
 Z|Y &\sim \text{Normal}(\mu = \mu_z(y), \sigma^2 = 1) \\
 X_1|Z, U &\sim \text{Normal}(\mu = \mu_{x_1}(z), \sigma^2 = 1) \\
 X_2|Z, U &\sim \text{Normal}(\mu = \mu_{x_2}(u), \sigma^2 = 1).
 \end{aligned} \tag{10}$$

For the confounded training and test sets, the parameters are given below:

$$\begin{aligned} q_y(u) &= \begin{cases} 0.2 & \text{if } u = 1 \\ 0.8 & \text{if } u = 2 \end{cases} & \mu_z(y) &= \begin{cases} -1.2 & \text{if } y = 1 \\ 1.2 & \text{if } y = 2 \end{cases} \\ \mu_{x_1}(z) &= \begin{cases} -1.8 & \text{if } z < 0 \\ 1.8 & \text{if } z > 0 \end{cases} & \mu_{x_2}(u) &= \begin{cases} -2.4 & \text{if } u = 1 \\ 2.4 & \text{if } u = 2 \end{cases}. \end{aligned} \quad (11)$$

Five thousand (5,000) samples are generated for the confounded training set, whereas 1,000 samples are generated for the confounded test set. With the confounder  $U$ , the generated positive samples (class 2) are more likely to concentrate in the positive region of  $X_2$ , by contrast with the non-confounded data. For the non-confounded test set, the confounding path between  $U$  and  $Y$  is disconnected by setting  $q_y(u) = 0.5$ , and 1,000 samples are generated. Consequently, the samples for two classes are optimally separated by the Bayes' boundary at  $X_1 = 0$ .

## A.2. Synthetic regression data

For the synthetic regression data, all variables are (multi-dimensional) Gaussian whose parameters may depend on their parent variables. Formally, their dependency is:

$$\begin{aligned} U &\sim \text{Normal}(\mu = 0, \sigma^2 = 1) \\ Y &= a_0 + a_1 U + \epsilon_Y \\ Z &= bY + \epsilon_Z \\ X &= c_0 U + c_1 Z + \epsilon_X. \end{aligned} \quad (12)$$

The generated confounded and non-confounded datasets have the same sample sizes as the synthetic classification data. The coefficients  $a_0 = 2$ ,  $a_1 = 1$ ,  $b = 1.5$ ,  $c_1 = 1$ ,  $c_0 = 5$  for the confounded setting and  $c_0 = 0$  for non-confounded setting.  $\epsilon_Y, \epsilon_Z, \epsilon_X \sim \text{Normal}(\mu = 0, \sigma^2 = 1)$  are a Gaussian noise term. In this case, the presence of the latent confounder  $U$  will lead to a smaller slope for the (linear) regression line. More specifically:

$$\begin{aligned} \hat{y}_{\text{conf}} &= 0.15x + 1.54 + \epsilon_1 \\ \hat{y}_{\text{unconf}} &= 0.67x + \epsilon_2. \end{aligned} \quad (13)$$

## A.3. Semi-synthetic background-MNIST data

To synthesise the background-MNIST dataset, we modify and embed the original handwriting digit images in the MNIST dataset into a front-door causal setting confounded by the background brightness. The following parametric data generation model is used:

$$\begin{aligned} U &\sim \text{Normal}(0, 5) \\ Y|U &\sim \text{Bernoulli}(p = q_y(u)) \\ Z|Y &\sim \text{Bernoulli}(p = r_z(y)) \\ \mathbf{X}|Z, U &\sim \text{MNIST}(z, u), \end{aligned} \quad (14)$$

where the Bernoulli parameter for  $Y$  is a function of the value of the confounder  $U$  given by:

$$q_y(u) = \frac{q^u}{q^u + (1-q)^u}, \quad (15)$$

where  $q = 0.8$  for confounded data. For  $q = 0.5$ , the data is non-confounded data because  $U$  imposes no effect on  $Y$ .  $\text{MNIST}(y, u)$  is a random function that retrieves a unique MNIST image  $\mathbf{x}$  representing digit "2" for  $y = 1$  and digit "6" for  $y = 2$ , and then the brightness of the selected image is converted by  $\mathbf{x} \mapsto \min(\mathbf{x} + \mathbf{v}(u), 255)$  where  $\mathbf{v}(u)$  is a same-shape matrix as the MNIST image whose value depends on  $u$ , that is:

$$v_{ij}(u) = 100 \times \left( \frac{1}{2} \arctan\left(\frac{1}{5}u\right) + \frac{1}{2} \right), \quad (16)$$

which maps the continuous confounder values onto the scaled background brightness values in the range  $[0, 100]$ .